Acoustic energy distribution in multi-component structures - Dynamical Energy Analysis versus numerically exact results

Gregor Tanner[1], **David Chappell**[1], **Hanya Ben Hamdin**[1], **Stefano Giani**[1], **Cathleen Seidel**[2], **and Frank Vogel**[2]

[1] School of Mathematical Sciences, University of Nottingham,
University Park, Nottingham NG7 2RD, UK
e-mail: **gregor.tanner@nottingham.ac.uk**

[2] inuTech GmbH, Fürther Str. 212, 90429 Nürnberg, Germany

Abstract

A new approach towards determining the distribution of mechanical and acoustic wave energy in complex built-up structures - also referred to as Dynamical Energy Analysis (DEA) - has been proposed recently (G Tanner, JSV 320, 1023 (2009)). The technique interpolates between "Statistical Energy Analysis" (SEA) and "ray tracing" containing both these methods as limiting cases. Within the new theory SEA is identified as a low resolution ray tracing algorithm and typical SEA assumptions can be quantified in terms of the properties of the ray dynamics. We have developed an efficient DEA code and have tested it for a range of multi-component model systems.

For reference purposes, we have undertaken numerically exact calculations for solving the underlying wave equations using both finite element (FEM) and boundary element (BEM) methods. The FEM calculations use sophisticated hp-adaptive discontinuous Galerkin methods. For the BEM calculations, we have developed a multi-component BEM solver for wave problems with variable wave speed and damping parameters across sub-systems.

1 Introduction

Distributions of mechanical or acoustic wave energy in complex built-up systems can in the high frequency limit often be modelled well by using thermodynamical or statistical approaches. The flow of wave energy is assumed to follow the gradient of the energy density just like heat energy flows along the temperature gradient [1]. To simplify the treatment, it is often suggested to partition the full system into subsystems and to assume that each subsystem is internally in thermal equilibrium. Interactions between directly coupled subsystems can then be described in terms of coupling constants determined by the properties of the wave dynamics at subsystem boundaries alone. These ideas form the basis of *Statistical Energy Analysis* (SEA) [2, 3].

A method similar in spirit but very different in applications is the so-called *ray tracing technique*. The wave intensity distribution at a specific point is determined by summing over contributions from all ray paths arriving at this point from a given source point - a method which has found widespread applications in room acoustics [4], seismology [5], wireless communications via radio waves [6] and computer imaging [7].

Ray tracing and SEA are in fact complimentary in many ways. Ray tracing provides a good model for wave problems where the effective number of reflections at walls or interfaces is relatively small and where detailed spatial resolution is required. SEA can handle complex structures carrying wave energy over many

subsystems including potentially a large number of reflections and scattering events, albeit at the cost of reduced resolution. In addition, the quality of SEA predictions may depend on the geometry of the subsystems, and error bounds are often hard to obtain. It can in fact be shown, that SEA is a low resolution ray tracing method [8]; ray tracing is in this sense superior to SEA, however, at a large additional computational cost [9]. Ray tracing and SEA both predict mean values of the energy distribution and omit information about wave effects such as interference or diffraction. Both methods are therefore expected to hold in the high frequency or small wavelength limit.

In this work, we discuss a method - *Dynamical Energy Analysis* (DEA) - which has recently been proposed in [8]. DEA interpolates between SEA and a full ray tracing analysis and thus enhances the range of applicability of standard SEA. Related methods have been discussed previously in the context of wave chaos [10] and structural dynamics [11]. In particular Langley's *Wave Intensity Analysis* (WIA) [12, 13] and Le Bot's thermodynamical high frequency boundary element method [14, 15] include details of the underlying ray dynamics. The approach employed here differs from these methods since multiple reflections are considered in terms of linear operators directly. Representing these operators in terms of basis function expansions then leads to SEA-type equations.

For reference purposes, we have done numerical calculations solving the wave problem exactly using FEM and BEM. We describe here in particular a multi-component boundary element method (MCBEM) well suited to deal for these type of wave problems. Our MCBEM approach uses boundary integral kernels for each sub-domain coupled through boundary conditions at the interface. A method for regularising hypersingular integral contributions will be presented.

The paper is structured as follows: in Sec. 2, we discuss the approximations necessary to reduce wave transport equations to flow equations, we introduce classical, linear flow operators in and derive the DEA equations. Some simple two-domain problems will be treated in Sec. 3 using the DEA method and FEM and BEM calculations.

2 Wave energy flow - outline of the theory

2.1 From the Green function to ray-flow equations

Throughout this paper we will focus on problems described by the Helmholtz equation with variable wave speed in different parts of the structure; examples are among others acoustics or vibrations of membranes. We will furthermore assume that the system is excited at a source point r_0 with a fixed angular frequency ω, that is, we seek the solution of the equation

$$\left(\nabla \frac{1}{m(r)} \nabla + \kappa\omega^2\right) G(r, r_0, \omega) = -\delta(r - r_0) \tag{1}$$

where $G(r, r_0, \omega)$ is the Green function, $m(r)$ is the local mass density and κ is a material parameter such as the adiabatic compressibility or the inverse tension. We assume furthermore that the system can be split into N sub-domains $\Omega_i, i = 1, \ldots, N$, in which the material parameters and thus the local wave speeds $c_j = \sqrt{m_j \kappa_j}$ are constant. Sub-system dependent damping is incorporated in this model through a complex-valued frequency term $\tilde{\omega}_j = \omega + i\mu_j c_j$ with μ_j the local damping parameter. The set of equations to be solved are thus

$$\left(\Delta + k_j^2\right) G(r, r_0, \omega) = -m_j\, \delta(r - r_0) \quad \text{for} \quad r \in \Omega_j \tag{2}$$

with local wave number $k_j = \tilde{\omega}/c_j$ and appropriate boundary conditions at the outer boundaries and the interfaces. The wave energy density at a point $r \in \Omega_j$ induced by the source is then proportional to the modulus-square of the Green function, that is,

$$\epsilon(r, r_0, \omega) \propto |G(r, r_0, \omega)|^2. \tag{3}$$

The linear wave equation (2) can in a natural way be associated with a ray dynamics via the Eikonal approximation, see for example [8]. Using small wave length asymptotics, one can write the Green function $G(r, r_0, \omega)$ in Eq. (1) as sum over all classical rays going from r_0 to r including reflections at the boundary. The wave energy density, Eq. (3), can then be expressed as a double sum over these ray paths where the dominant terms (often denoted the *diagonal terms*) originate from the modulus square of single orbit contributions giving rise to a smooth background signal. The *off-diagonal part* is responsible for fluctuations of the signal due to (overlapping) resonances.

It has been shown in [8] that the background part can be obtained by a ray tracing treatment. That is, the smooth part of the Green function can be described in terms the flow of 'fictitious' non-interacting particles emerging from the source point r_0 uniformly in all directions and propagating along ray trajectories. The corresponding ray density $\rho(r, r_0, \omega)$ is then given as

$$\rho(r, r_0, \omega) = \left\langle |G(r, r_0, \omega)|^2 \right\rangle,$$

where the average is for example taken over frequency ranges or over 'similar' systems. This makes it possible to relate wave energy densities to classical flow equations and thus thermodynamical concepts which are at the heart of an SEA treatment. This connection has also be highlighted in [16, 17]. In DEA, the classical flow is determined in terms of linear *phase space operators* [8]. We adopt a boundary mapping approach in what follows, that is, we describe the flow operators in terms of boundary operators which leads in a natural way to substructuring and SEA-type equations.

2.2 Linear phase space operators and DEA

We sketch here the derivation of the DEA flow equations; for details see [8]. The time dependence of a density of ray trajectories can be described in terms of a linear phase space operator $\mathcal{L}^\tau(X, Y) = \delta(X - \varphi^\tau(Y))$, known as a Perron-Frobenius operator in dynamical systems theory, such that,

$$\rho(X, \tau) = \int \mathcal{L}^\tau(X, Y)\rho_0(Y)dY. \tag{4}$$

Here $X = (r, p)$ denotes the phase space coordinate with position vector r and momentum (or velocity) vector p. The phase space flow $\varphi^\tau(Y)$ gives the position of the particle after time τ starting at $Y = (r', p')$ when $\tau = 0$. Furthermore, ρ_0 denotes the initial ray density at time $\tau = 0$ in phase space and the domain of integration is over the whole of phase space.

Consider a source localised at a point r_0 emitting waves continuously at a fixed angular frequency ω. Standard ray tracing techniques estimate the wave energy at a receiver point r by determining the density of rays starting at r_0 and reaching r after some unspecified time. This may be written in the form

$$\rho(r, r_0, \omega) = \int_0^\infty d\tau \int dp \int dY\, w(Y, \tau)\mathcal{L}^\tau(X, Y)\rho_0(Y, \omega), \tag{5}$$

with initial density $\rho_0(Y, \omega) = \delta(r' - r_0)\delta(\omega^2 - H(Y))$, where H is the Hamilton function corresponding to the wave operator in (2). It can be shown that equation (5) is equivalent to the diagonal approximation [8]. A weight function w is included to incorporate damping and reflection/ transmission coefficients. It is assumed that w is multiplicative, that is, $(w(\varphi^{\tau_1}(X), \tau_2)w(X, \tau_1) = w(X, \tau_1 + \tau_2))$, which holds for standard absorption mechanism and reflection processes.

In order to solve the stationary flow problem (5), a boundary mapping technique is employed. For the time being let us consider a problem with a single (sub-)system $\Omega = \Omega_1$ with boundary Γ. The following three step procedure will be used, see Fig. 1: firstly, the ray density emanating continuously from the source is mapped onto the boundary Γ. The resulting boundary layer density $\rho_\Gamma^{(0)}$ is equivalent to a source density on the boundary producing the same ray field in the interior as the original source field after one

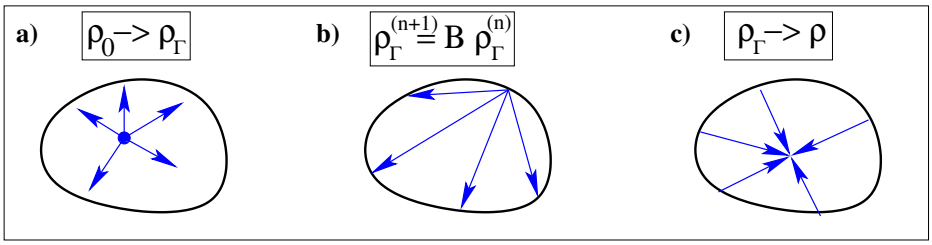

Figure 1: a) Mapping from source distribution to boundary distribution; b) mapping under boundary operator $\mathcal{B}$; c) mapping from boundary distribution into interior

reflection. Secondly, densities on the boundary are mapped back onto the boundary by a boundary operator $\mathcal{B}(X^s, Y^s; \omega) = w(Y^s)\delta(X^s - \phi^\omega(Y^s))$, where $X^s = (s, p_s)$ represents the coordinates on the boundary (s parametrises Γ and p_s denotes the momentum component tangential to Γ at s), likewise $Y^s = (s', p'_s)$, and ϕ^ω is the invertible boundary map. Note that convexity is assumed to ensure ϕ^ω is well defined; non-convex regions could be handled by introducing a cut-off function in the shadow zone [15].

The stationary density on the boundary induced by the initial boundary distribution $\rho_\Gamma^{(0)}(X^s, \omega)$ can then be obtained using

$$\rho_\Gamma(\omega) = \sum_{n=0}^{\infty} \mathcal{B}^n(\omega)\rho_\Gamma^{(0)}(\omega) = (I - \mathcal{B}(\omega))^{-1}\rho_\Gamma^{(0)}(\omega), \tag{6}$$

where $\mathcal{B}^n$ contains trajectories undergoing n reflections at the boundary. Thirdly, the resulting density distribution on the boundary, $\rho_\Gamma(X^s, \omega)$, is mapped back into the interior region. One obtains the density (5) after projecting down onto coordinate space.

2.3 Basis representation

To evaluate $(1 - \mathcal{B})^{-1}$ it is convenient to express the operator $\mathcal{B}$ in a suitable set of basis functions defined on the boundary. Depending on the topology of the boundary, complete function sets such as a Fourier basis for two dimensional domains, a Chebyshev basis for enclosures with corners or spherical harmonics for bodies in three dimensions may be chosen. Denoting the orthonormal basis $\{\ldots, \Psi_0, \Psi_1, \Psi_2, \ldots\}$, we obtain

$$\begin{aligned} B_{nm} &= \int dX_s dX'_s \, \Psi_n^*(X_s)\, \mathcal{B}(X_s, X'_s; \omega)\, \Psi_m(X'_s) \\ &= \int dX'_s \, \Psi_n^*(\phi_\omega(X'_s))\, w(X'_s)\, \Psi_m(X'_s)\,. \end{aligned} \tag{7}$$

The treatment is reminiscent to the Fourier-mode approximation in the wave intensity analysis (WIA) [12, 13]; note, however, that the basis functions cover both momentum and position space here and can thus resolve spacial density inhomogeneities unlike WIA. For more details, see again [8].

So far, we have sketched the method for a single cavity problem. Moving to multi-component problems as outlined above, we need to consider the dynamics including rays travelling from one subsystem to another. Subsystem boundaries are typically surfaces of reflection/transmission due to sudden changes in the material parameters. We thus describe the full dynamics in terms of the subsystem boundary operators $\mathcal{B}^{ij}$; for adjacent subsystems, power flowing from domain Ω_j to Ω_i is then described through the operator

$$\mathcal{B}^{ij}(X_s^i, X_s^j) = w^{ij}(X_s^j)\, \delta(X_s^i - \phi_\omega^{ij}(X_s^j)) \tag{8}$$

where ϕ_ω^{ij} is the boundary map in subsystem j mapped onto the boundary of the adjacent subsystem i and X_s^i are the coordinates of subsystem i. The weight w^{ij} contains, among other factors, reflection and transmission coefficients characterising the coupling at the interface between Ω_j and Ω_i.

A basis function representation of the full operator $\mathcal{B}$ as suggested in Eq. (7) is now written in terms of subsystem boundary basis functions Ψ_n^i with

$$B_{nm}^{ij} = \int dX_s^i dX_s^j \, \Psi^{i*}{}_n(X_s^i) \, \mathcal{B}^{ij}(X_s^i, X_s^j) \, \Psi_m^j(X_s^j). \tag{9}$$

The equilibrium distribution on the boundaries of the subsystems is obtained by solving the systems of equations (6) for the multi-component operator, that is,

$$(1 - B)\rho_\Gamma = \rho_\Gamma^0 \, . \tag{10}$$

Here, B is the full operator including all subsystems and the equation is solved for the unknown energy densities $\rho_\Gamma = \{\rho_{\Gamma_i}, i = 1, \ldots N\}$, where ρ_{Γ_i} denotes the coefficients with respect to the basis function representation of the density on the boundary of subsystem i.

2.4 DEA - from ray tracing to SEA

The various representations given so far are all equivalent and correspond to a description of the wave dynamics in terms of the ray tracing ansatz (5). Traditional ray tracing based on sampling ray solutions over the available phase space is rather inefficient, however. Convergence tends to be fairly slow, especially if absorption is low and an exponentially increasing number of long paths including multiple reflections need to be taken into account.

An SEA-type treatment emerges when approximating the individual operators $\mathcal{B}^{ij}$ by the lowest order basis function only, in general the constant function $\Psi_0^j = (A_\Gamma^j)^{-1/2}$ with A_Γ^j, the area/length of the boundary of Ω_j. (Note that for a Chebyshev polynomial basis representation, which has been used in actual numerical calculations in Sec. 3.2, basis functions are multiplied by a weight function, which needs to be omitted to obtain the SEA results.) The matrix B^{ij} is then one-dimensional and gives the mean transmission rate from subsystem Ω_j to Ω_i. It is thus equivalent to the coupling loss factor η_{ij} used in standard SEA equations. The resulting full N-dimensional B matrix (with N, the number of subsystems) yields a set of SEA equations using the relation (10).

An SEA approximation is justified if the ray dynamics within each subsystem is sufficiently chaotic such that a trajectory entering subsystem i 'forgets' everything about its past history before exciting Ω_i again. In other words, correlations within the dynamics must decay fast on the time scales of the staying time, that is, the time scale it takes for a typical ray to leave the cavity Ω_i. These conditions will be fulfilled if the subsystems' boundaries are sufficiently irregular, the subsystems are dynamically well separated and absorption and dissipation is small - conditions typically cited in an SEA context. In this case, SEA is an extremely efficient method compared to standard ray tracing techniques. However, for subsystems with regular features, such as rectangular cavities or corridor-like elements, incoming rays are directly channelled into outgoing rays thus violating the equilibration hypothesis and introducing memory effects. Likewise, strong damping may lead to a significant decay of the signal before reaching the exit channel introducing geometric (system dependent) effects.

These features can be incorporated in DEA by including higher order basis functions for each subsystem boundary operator B^{ij}. This leads to a smooth interpolation from SEA to a full ray-tracing treatment. The maximal number of basis functions needed to reach convergence are expected to be relatively small thus making the new method more efficient than a full ray tracing treatment - in particular in the small damping regime.

3 A numerical example: coupled two-domain systems

The method has been implemented numerically for a coupled two-domain system; the wave energy distribution has been calculated using DEA and compared to the numerically exact solutions obtained from an advanced hp-adaptive FEM method and from a multi-component BEM treatment.

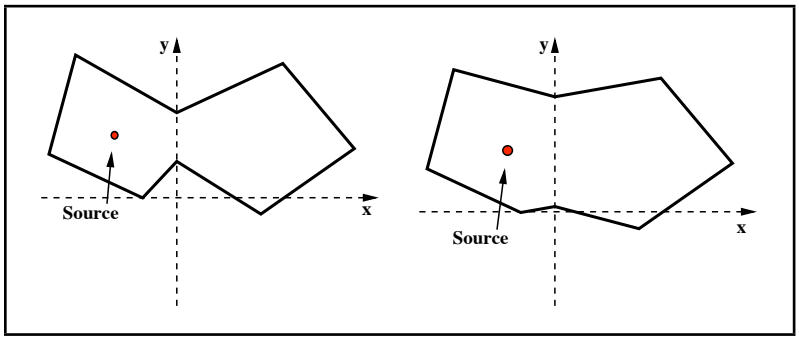

Figure 2: Coupled two-domain systems named configurations A and B, respectively.

In the following, we restrict the analysis to 2D problems and to two-domain systems such as depicted in Fig. 2 with a source point r_0 in the interior of the left domain and homogeneous Dirichlet or Neumann boundary conditions on the outer boundaries. We furthermore assume that the wave velocity is constant within each sub-domain, but may jump discontinuously at the interface between the two domains giving rise to reflection/transmission phenomena. The FEM method has been described elsewhere in detail [18, 19, 20], see in particular [21] for applications to wave equations. We will thus focus here on a brief description of BEM for multi-component systems with variable wave speed. BEM and FEM solutions will be compared to DEA result at the end of this section.

3.1 Multi-component boundary element method - MCBEM

In this section, we will briefly sketch the main steps for deriving a multi-component BEM; a detailed description will be given elsewhere [22]. We will focus here on two-domain, 2D problems such as shown in Fig. 2; we assume that both the wave speed and absorption coefficients may change discontinuously at the interface between the left (region 1) and right (region 2) hand side.

An integral part of the BEM is the knowledge of the free solution of Eq. (2) in the interior disregarding boundaries. While analytic solution for a free Green function incorporating a jump at a single interface can be derived in principle, the intention here is to devise a method for multi-component systems, where such a treatment would become impractical. We thus construct a BEM kernel for each subdomain separately and introduce a coupling at the interfaces. The free Green function solving Eq. (2) in domain Ω_j is given as

$$G_0(r, r_0; k_j) = m_j \frac{i}{4} H_0^{(1)}(k_j |r - r_0|) \tag{11}$$

where H_0 is the zeroth order Hankel function and $k_j = \omega/c_j + i\mu_j$, $j = 1, 2$ with μ_j, the damping parameter and m_j are the material densities in the sub-domain Ω_j.

We thus split the boundary of domain $j = 1, 2$ into an outer part Γ_j and a part comprising the interface I. Using standard boundary element techniques, one arrives at an integral equation on the boundary of the form

$$\int_{\Gamma_j \cup I} \left[G_0(q, r, k_j) \frac{\partial G_j(q, r_0)}{\partial n} - G_j(q, r_0) \frac{\partial G_0(q, r, k_j)}{\partial n} \right] dq = -\delta_{1,j}\, G_0(r, r_0, k_j) + G_j(r, r_0), \tag{12}$$

where we assume that the source is in region 1, i.e. $r_0 \in \Omega_1$.

We will assume Dirichlet boundary conditions on Γ_j, that is, $G_j(q, r_0; \omega) = 0$ for $q \in \Gamma_j$. The continuity of the Green function and conservation of the energy flux along the interface require in addition

$$\left.\begin{array}{rcl} G_1(q, r_0) & = & G_2(q, r_0) \\ \frac{1}{m_1}\, \partial G_1(q, r_0)/\partial n & = & -\frac{1}{m_2}\, \partial G_2(q, r_0)/\partial n \end{array}\right\}, \quad \text{for} \quad q \in I \tag{13}$$

where$\partial/\partial n$ denotes the outward normal derivative with respect to the first argument. After taking the normal derivative with respect to the variable r (suitably extending the notion of a normal derivative into the interior of Ω_j) and then taking the limit $r \to \beta \in \Gamma_j \cup I$ and writing

$$\mu_j(q, r_0) = \frac{\partial G_j(q, r_0)}{\partial n},$$

one arrives at the set of equations

$$\begin{aligned}
&\text{for } \beta \in \Gamma_j \\
&\qquad \int_I \left[\frac{\partial G_0(q,\beta,k_j)}{\partial n_\beta} \mu_{j,I}(q,r_0) - G_{j,I}(q,r_0) \frac{\partial^2 G_0(q,\beta,k_j)}{\partial n_\beta \partial n_q} \right] dq \\
&+ \int_{\Gamma_j} \frac{\partial G_0(q,\beta,k_j)}{\partial n_\beta} \mu_j(q,r_0) dq = -\delta_{1,j} \frac{\partial G_0(\beta,r_0,k_j)}{\partial n_\beta} + \frac{1}{2}\mu_j(\beta,r_0) \qquad (14) \\
&\text{for } \beta \in I \\
&\qquad \int_I \frac{\partial G_0(q,\beta,k_j)}{\partial n_1} \mu_{j,I}(q,r_0) dq - \frac{\partial}{\partial n_\beta} \int_I G_{j,I}(q,r_0) \frac{\partial G_0(q,\beta,k_j)}{\partial n_q} dq \\
&+ \int_{\Gamma_j} \frac{\partial G_0(q,\beta,k_j)}{\partial n_\beta} \mu_j(q,r_0) dq = -\delta_{j,\beta} \frac{\partial G_0(\beta,r_0,k_j)}{\partial n_\beta} + \frac{1}{2}\mu_j(\beta,r_0), \qquad (15)
\end{aligned}$$

which are coupled through the boundary conditions Eq. (13).

Note, that the 2nd derivative of G_0 does have a 1 $|\beta - q|^2$ singularity, and exchanging integration and differentiation is not possible in the first line of Eq. (15). A careful treatment of this hyper-singular term leads to the following formula

$$\lim_{\Delta r \to 0} \int_0^{q_1} \frac{\partial^2 G_0(r,q)}{\partial n_\beta \partial n_q} dq = k^2 \int_0^{q_1} G_0(q,\beta,k) dq + \left. \frac{d}{dq} G_0(q,\beta,k) \right|_{q_1}. \qquad (16)$$

Using this singularity free expression, see [23] for a 3D treatment, together with standard collocation method [24] leads to a singularity free set of equations.

By choosing N_{Γ_j} and N_I points equidistantly on the boundary Γ_j and the interface I, respectively, one arrives at a matrix equation for the $N = N_{\Gamma_1} + N_{\Gamma_2} + 4N_I$ unknowns, namely, the vector

$$Q = \{\mu_1, \mu_{1,I}, G_{1,I}, \mu_2, \mu_{2,I}, G_{2,I}\}$$

and

$$\begin{bmatrix}
\mathbf{K}_{\Gamma_1\Gamma_1} & \mathbf{F}_{\Gamma_1 I_1} & \mathbf{G}_{\Gamma_1 I_1} & \mathbf{0} & \mathbf{0} & \mathbf{0} \\
\mathbf{F}_{I_1\Gamma_1} & \mathbf{K}_{I_1 I_1} & \mathbf{G}_{I_1,I_1} & \mathbf{0} & \mathbf{0} & \mathbf{0} \\
\mathbf{0} & \frac{1}{m_1}\mathbf{I} & -\mathbf{I} & \mathbf{0} & \frac{1}{m_2}\mathbf{I} & \mathbf{I} \\
\mathbf{0} & \mathbf{0} & \mathbf{0} & \mathbf{K}_{\Gamma_2\Gamma_2} & \mathbf{F}_{\Gamma_2 I_2} & \mathbf{G}_{\Gamma_2 I_2} \\
\mathbf{0} & \mathbf{0} & \mathbf{0} & \mathbf{F}_{I_2\Gamma_2} & \mathbf{K}_{I_2 I_2} & \mathbf{G}_{I_2 I_2} \\
\mathbf{0} & \frac{1}{m_1}\mathbf{I} & \mathbf{I} & \mathbf{0} & \frac{1}{m_2}\mathbf{I} & -\mathbf{I}
\end{bmatrix}
\begin{bmatrix} \mu_1 \\ \mu_{1,I} \\ G_{1,I} \\ \mu_2 \\ \mu_{2,I} \\ G_{2,I} \end{bmatrix}
=
\begin{pmatrix} \underline{B}_{\Gamma_1} \\ \underline{B}_{I_1} \\ 0 \\ 0 \\ 0 \\ 0 \end{pmatrix}$$

with

$$\mathbf{K}_{\Gamma_1\Gamma_1}(i,j) \;=\; \left[2\frac{\partial G_0(q_i,q_j,k_1)}{\partial n_j} - \delta_{ij} \right] \Delta q, \qquad q_i, q_j \in \Gamma_1 \qquad (17)$$

$$\mathbf{F}_{\Gamma_1 I_1}(i,j) = 2\frac{\partial G_0(q_i,q_j,k_1)}{\partial n_j}\Delta q, \qquad q_j \in \Gamma_1, q_i \in I_1 \tag{18}$$

$$\mathbf{G}_{\Gamma_1 I_1}(i,j) = -2\frac{\partial^2 G_0(q_i,q_j,k_1)}{\partial n_i \partial n_j}\Delta q, \qquad q_j \in \Gamma_1, q_i \in I_1 \tag{19}$$

$$\mathbf{F}_{I_1 \Gamma_1}(i,j) = 2\frac{\partial G_0(q_i,q_j,k_1)}{\partial n_j}\Delta q, \qquad q_i \in \Gamma_1, q_j \in I_1 \tag{20}$$

$$\mathbf{K}_{I_1 I_1}(i,j) = \left[2\frac{\partial G_0(q_i,q_j,k_1)}{\partial n_j} - \delta_{ij}\right]\Delta q, \qquad q_i, q_j \in I_1 \tag{21}$$

$$B_{\Gamma_1}(j) = -2\frac{\partial G_0(q_j,\mathbf{r}',k_1)}{\partial n_j}, \qquad q_j \in \Gamma_1 \tag{22}$$

$$B_{I_1}(j) = -2\frac{\partial G_0(q_j,\mathbf{r}',k_1)}{\partial n_j}, \qquad q_j \in I_1 \tag{23}$$

$$\mathbf{G}_{I_1,I_1}(i,j) = \begin{cases} -2\left[k_1^2 F(\Delta q) - \frac{\imath k_1}{2} H_1^{(1)}\left(\frac{k_1 \Delta q}{2}\right)\right], & \text{if } q_i = q_j; \\ -2\frac{\partial^2 G_0(q_i,q_j,k_1)}{\partial n_j \partial n_i}\Delta q, & \text{if } q_i \neq q_j. \end{cases} \tag{24}$$

with Δq, the distance between points on the boundary and $F(\Delta q)$ represents the integral over the free Green function in Eq. (16). Here, $\mathbf{K}_{\Gamma_1\Gamma_1}$ contains rays segments starting and ending on the boundary Γ_1, $\mathbf{F}_{\Gamma_1 I_1}$ has contributions from rays starting on γ_1 and hitting the interface, $\mathbf{G}_{I_1,I_1}$ contains contributions from the interface to itself, and similarly for the other matrices.
The matrices on the fourth and fifth row have the same structure as the ones on the first and the second row, apart from a change of the wavenumber. From the solution vector, we can easily compute the Green function at any interior point in the coupled polygonal domain using Eq. (12). Some example solutions are shown in Fig. 3.

3.2 Wave solutions compared to DEA and SEA - results

We consider coupled two-domain systems as shown in Figs. 2 and 3. Configuration A features irregular shaped, well separated pentagonal subsystems and thus SEA is expected to work well. In configuration B, the size of the interface between the sub-systems is increased reducing their dynamical separation and therefore the applicability of SEA.

In the examples here the calculations have been performed with the wave-speed fixed to unity in both subsystems, that is, $c_1 = c_2 = 1$. Finite basis sets have been employed with basis functions of the same order (N) for position and momentum in both subsystems. This gives rise to matrices of size $\dim B = (N+1)^2(N_1+N_2)$, where $N_i - 1$ is the number of geometric refinements in subsystem i. Energy distributions have been studied as a function of the frequency with a hysteretic damping factor $\eta = 0.01$, where $\mu_i = k_i\eta/2$ for $i = 1, 2$.

Results for the ratios of the total energy in each subsystem are shown in Figs. 4 and 5. Here the dotted lines represent solutions computed using FEM and BEM at a range of frequencies ± 5Hz around the frequencies used for the SEA and DEA computations. Note that the damping is fixed to the value employed for the central (SEA/DEA) frequency. Fast convergence with increasing basis size is evident in each case. It is also clear that SEA works reasonably well for configuration A since the SEA prediction is close to that from DEA and within the range of FEM/BEM solution values. In particular the SEA prediction is good for lower damping values (i.e. lower frequencies). As expected, the SEA prediction diverges from both the FEM and DEA predictions in configuration B. The versatility and efficiency of the Chebyshev approximation with Gauss-Chebyshev quadrature will be demonstrated in the presentation by considering some different and more complex built-up systems.

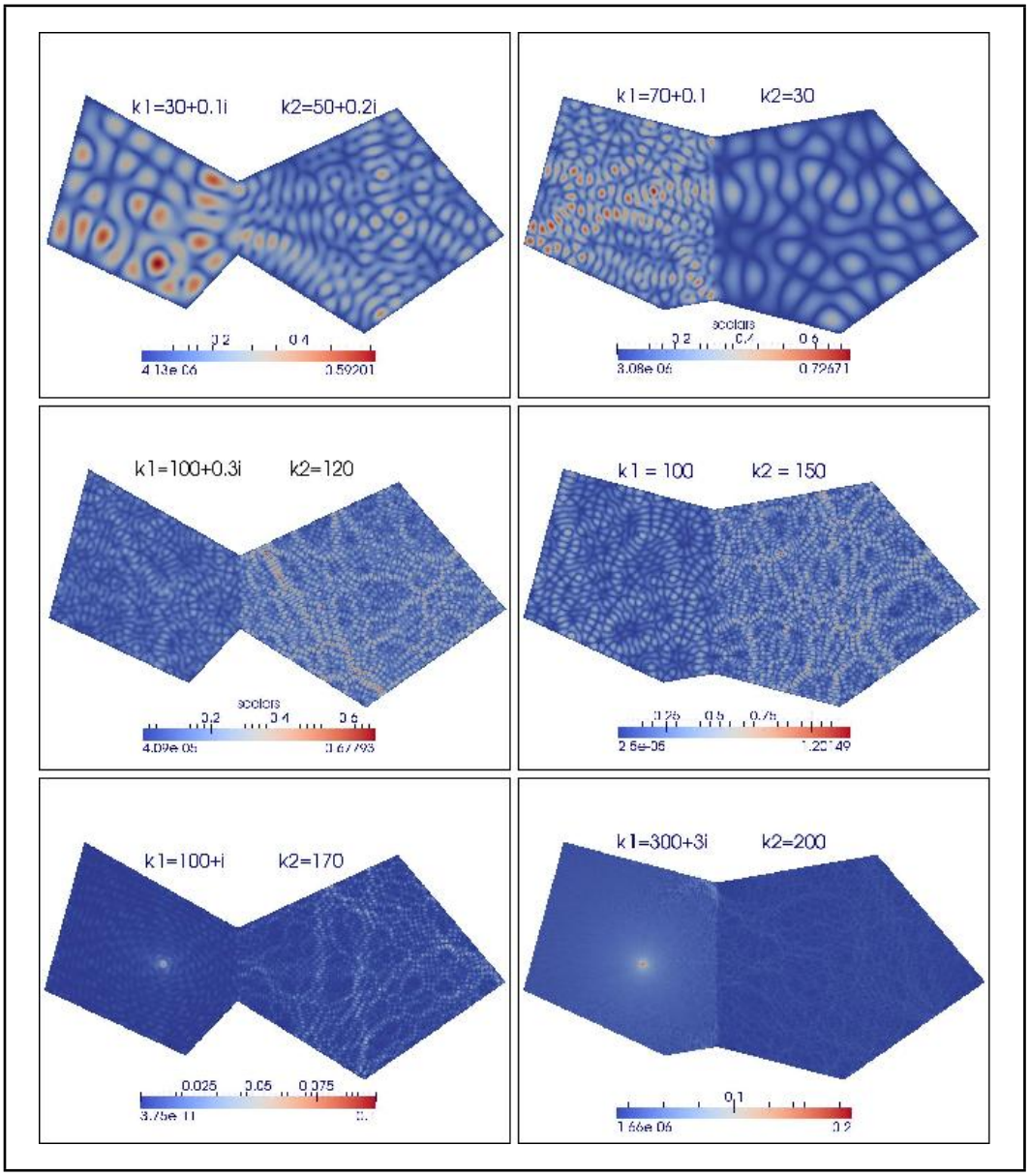

Figure 3: Greens function for coupled domains at different wave numbers and damping parameters.

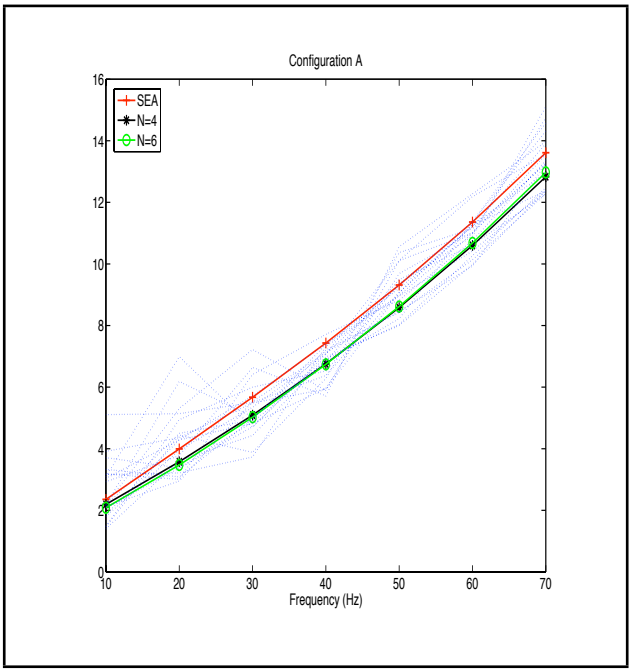

Figure 4: Ratio of total energies $\|G_1\|^2/\|G_2\|^2$ in config. A.

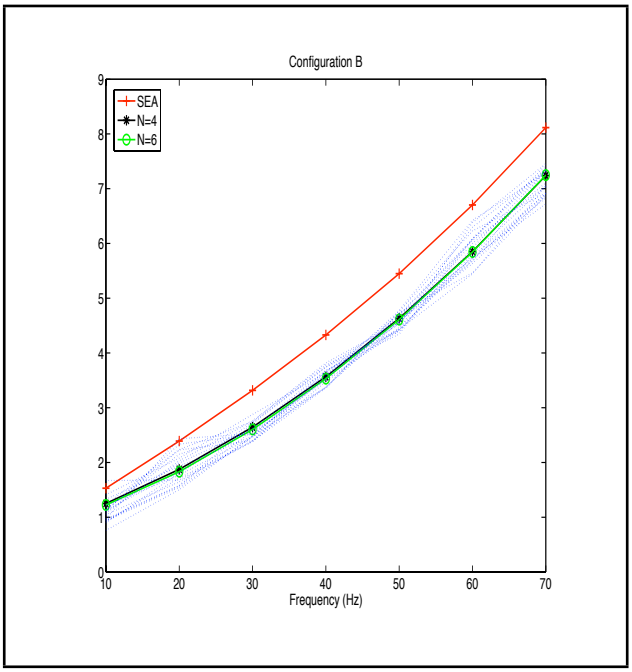

Figure 5: Ratio of total energies $\|G_1\|^2/\|G_2\|^2$ in config. B.

4 Conclusions

We have shown that ray tracing methods and SEA are closely related and that the latter is indeed an approximation of the former by smoothing out the details of ray dynamics within individual subsystems. We propose a numerical technique which interpolates between SEA and full ray tracing by resolving the ray dynamics on a finer and finer scale. This is achieved by expressing the dynamics in terms of linear boundary operators and representing those in terms of a set of basis functions on the boundary. The resolution of the dynamics is now determined by the number of boundary functions taken into account.

We have tested the new method for two two coupled domain models and compared the results with FEM and BEM calculations. We found that DEA accounts correctly for correlations in the underlying ray dynamics and applies in situations where standard SEA shows systematic deviations from the FEM/BEM solutions. DEA is thus a more universal tool to predict average energy distributions at a small computational overhead.

5 ACKNOWLEDGEMENT

Support from the EPSRC (grant EP/F069391/1) and the EU (FP7IAPP grant MIDEA) is gratefully acknowledged.

References

[1] *Statistical analysis of power injection and response in structures and rooms*, Lyon R H 1969 *Journal of the Acoustical Society of America* **45** 545

[2] Lyon R H and DeJong R G 1995 *Theory and Application of statistical energy analysis* (2nd edn. Boston, MA: Butterworth-Heinemann)

[3] Craik R J M 1996 *Sound transmission through buildings: using statistical energy analysis* (Gower, Hampshire)

[4] Kuttruff H 2000 *Room Acoustics*, 4th edition, Spon Press, London

[5] Cervený V 2001 *Seismic Ray Theory* (Cambridge University Press)

[6] Mc Kown J W and Hamilton Jr R L 1991 *Ray Tracing as a Design Tool for Radio Networks*, IEEE Network Magazine 27

[7] Glasser A S (Ed) 1989 *An Introduction to Ray Tracing* (Academic Press)

[8] *Dynamical energy analysis - Determining wave energy distributions in vibro-acoustical structures in the high-frequency regime* Tanner G 2009 *Journal of Sound and Vibration* **320** 1023

[9] *Vibrations in several interconnected regions: a comparison of SEA, ray theory and numerical results*, Kulkarni S, Leppington F G and Broadbent E G 2001 *Wave Motion* **33** 79

[10] *Wave chaos in acoustics and elasticity*, Tanner G and Søndergaard N 2007 *Journal of Physics A* **40** R443

[11] *Advanced Statistical Energy Analysis*, Heron K H 1994 *Philosophical Transactions of the Royal Society London A* **346** 501.

[12] *A wave intensity technique for the analysis of high frequency vibrations*, Langley R S 1992 *Journal of Sound and Vibration* **159** 483

[13] *Wave Intensity Analysis of High Frequency Vibrations*, Langley R S and Bercin A N 1994 *Philosophical Transactions of the Royal Society London A* **346** 489.

[14] *A vibroacoustic model for high frequency analysis*, Le Bot A 1998 *Journal of Sound and Vibration* **211** 537

[15] *Energy transfer for high frequencies in Built-up structures*, Le Bot A 2002 *Journal of Sound and Vibration* **250** 247

[16] *Derivation of statistical energy analysis from radiative exchanges*, Le Bot A 2007 *Journal of Sound and Vibration* **300** 763

[17] *Entropy in statistical energy analysis*, Le Bot A 2009 *J Acoust Soc Am* **125** 1473

[18] *Unified analysis of discontinuous Galerkin methods for elliptic problems*, Arnold D N, Brezzi F, Cockburn B and Marini L D 2001 *SIAM J. Numer. Anal.* **39(5)** 1749

[19] *An Optimal Order Interior Penalty Discontinuous Galerkin Discretization of the Compressible Navier–Stokes Equations*, Hartmann R and Houston P 2008 *J. Comp. Phys.* **227** 9670

[20] *Energy Norm A Posteriori Error Estimation of hp–Adaptive Discontinuous Galerkin Methods for Elliptic Problems*, Houston P, Schötzau D and Wihler T P 2007 *M3AS* **17(1)** 33

[21] *Wave transport in complex vibro-acoustic structures in the high frequency limit*, to appear in the *Proceedings of IUTAM2009, St Petersburg, 2009*

[22] *A multi-component boundary element method in two dimensions*, Ben Hamdin H and Tanner G, preprint (2010)

[23] *Boundary integral solutions of three dimensional acoustic radiation problems*, Meyer W L, Bell W A, and Zinn B T 1978 *J. Sound. Vib.***59** 245

[24] *Modelling The Transient Interaction Of An Elastic Structure With An Exterior Acoustic Field*, Chappell D J 2007, PhD Thesis, Brighton University